Supporting Information

Rathour and Narayanan 10.1073/pnas.1316599111

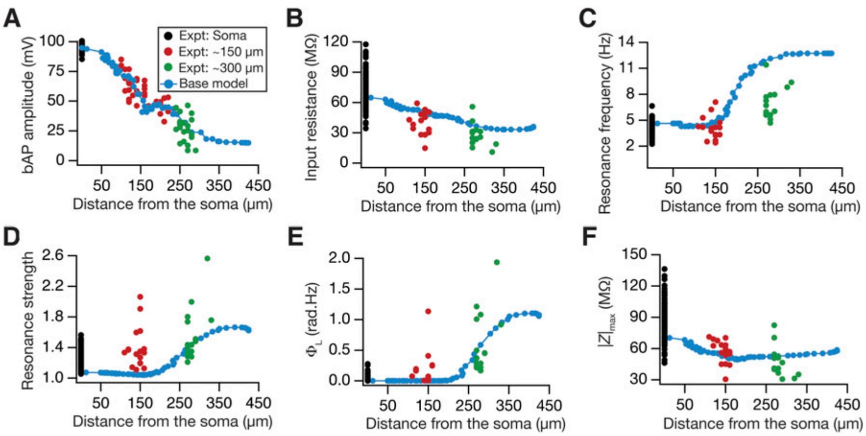

Fig. S1. The six functional maps in the base model match with corresponding experimental data. (*A–F*) Functional map of back-propagating action potential (bAP) (*A*), input resistance (R_{in}) (*B*), resonance frequency (f_R) (*C*), resonance strength (*Q*) (*D*), total inductive phase (Φ_L) (*E*), and maximum impedance amplitude ($|Z|_{max}$) (*F*) in the base model overlaid with corresponding experimental data. $n = 28$ (soma), 35 (~150 μm), and 30 (~300 μm) for *A*, and $n = 121$ (soma), 17 (~150 μm), and 15 (~300 μm) for *B–F*. The color codes for all panels follow the annotation provided in *A*; black, red, and green markers refer to experimental data (plotted with respective to corresponding distance values) at the soma, ~150 μm, and ~300 μm (compare Table S2); blue markers along with the solid line refer to the values obtained from the base model (same as corresponding plots in Fig. 1 *F–H*). The base model was obtained with default parameters mentioned in Table S1.

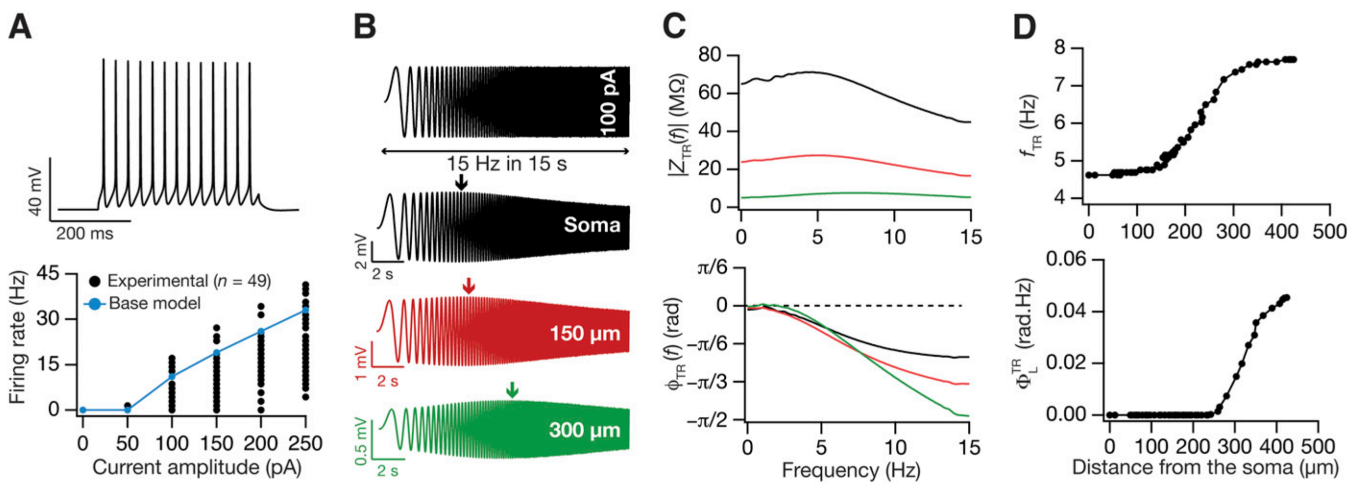

Fig. S2. Evaluation of unconstrained measurements in the base model. (*A*) *Upper*, action potential traces in response to 250-pA somatic current injection for 400 ms. *Lower*, somatic firing rate profile (*f–I* curve) in the base model (blue) overlaid with experimental *f–I* data (black) obtained from the CA1 pyramidal neurons. (*B*) A chirp current stimulus, 100 pA (peak-to-peak) in amplitude and frequency increasing linearly from 0.1 Hz to 15 Hz in 15 s (*Upper*), was injected at different locations, soma (black), ~150 μm (red), and ~300 μm (green), to get corresponding voltage responses at the soma (*Lower*). (*C*) Impedance amplitude profile [$|Z|_{TR}(f)$] (*Upper*) and impedance phase profile [$\phi_{TR}(f)$] (*Lower*) obtained from the voltage response to the chirp stimulus, shown in *B*. (*D*) Functional map corresponding to transfer resonance frequency (f_{TR}) (*Upper*) and transfer total inductive phase Φ_L^{TR} (*Lower*) along the trunk. Note that the base model was constrained for physiological properties in Fig. 1 and measurements here matched with their experimental counterparts, without being explicitly constrained.

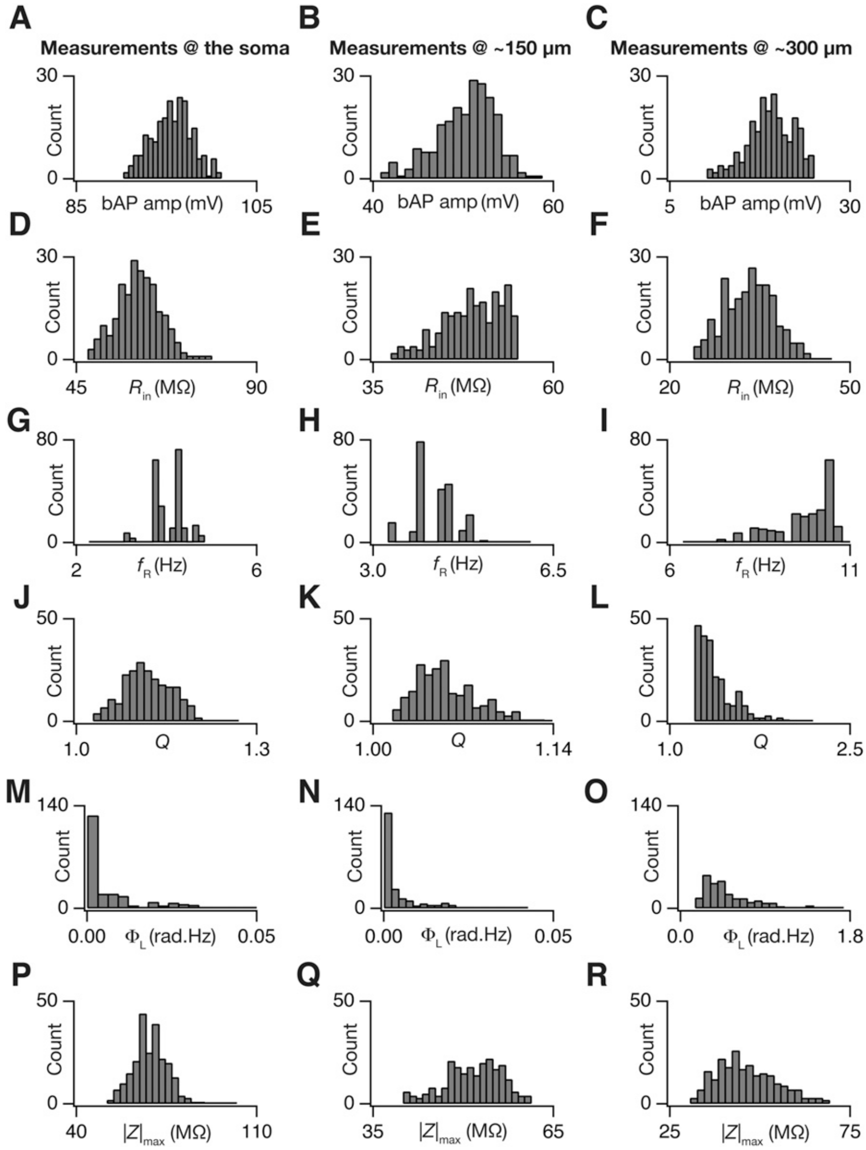

Fig. S3. Distribution of physiologically relevant measurements in the population of valid neuronal models at different locations. (*A*–*C*) Distribution of back propagation of action potential (bAP) amplitude in the population of valid models at the soma (*A*), ∼150 μm (*B*), and ∼300 μm (*C*). (*D*–*F*) Distribution of input resistance, R_{in}, in the population of valid models at the soma (*D*), ∼150 μm (*E*), and ∼300 μm (*F*). (*G*–*I*) Distribution of resonance frequency f_R, in the population of valid models at the soma (*G*), ∼150 μm (*H*), and ∼300 μm (*I*). (*J*–*L*) Distribution of resonance strength, *Q*, in the population of valid models at the soma (*J*), ∼150 μm (*K*), and ∼300 μm (*L*). (*M*–*O*) Distribution of total inductive phase, Φ_L, in the population of valid models at the soma (*M*), ∼150 μm (*N*), and ∼300 μm (*O*). (*P*–*R*) Distribution of maximum impedance amplitude, $|Z|_{max}$, in the population of valid models at the soma (*P*), ∼150 μm (*Q*), and ∼300 μm (*R*). For all panels $n = 228$.

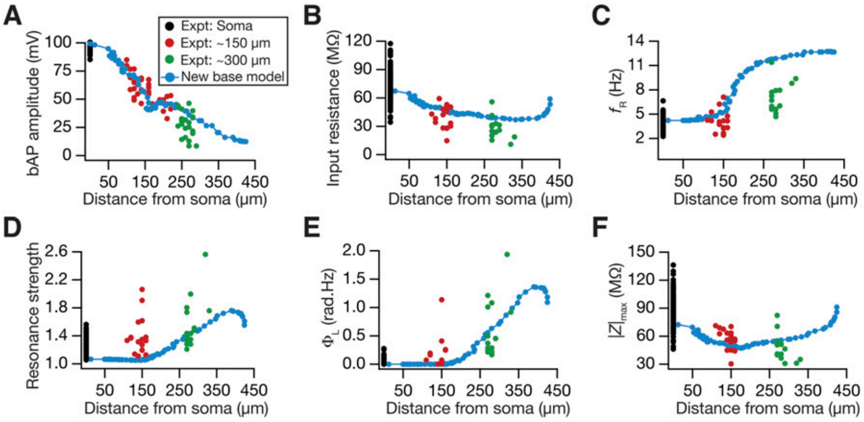

Fig. S4. The six functional maps in the new base model match with corresponding experimental data. (*A*–*F*) Functional map of back-propagating action potential (bAP) (*A*), input resistance (R_{in}) (*B*), resonance frequency (f_R) (*C*), resonance strength (*Q*) (*D*), total inductive phase (Φ_L) (*E*), and maximum impedance amplitude ($|Z|_{max}$) (*F*) in the new base model overlaid with corresponding experimental data (same as Fig. S1 for the base model). The color codes for all panels follow the annotation provided in *A*; black, red, and green markers refer to experimental data (plotted with respect to corresponding distance values) at the soma, ∼150 µm, and ∼300 µm (compare Table S2); blue markers along with the solid line refer to the values obtained from the new base model. The new base model was obtained by altering gradients in the intracellular resistivity, the specific membrane resistance, and the conductances of the hyperpolarization-activated cyclic-nucleotide-gated, *A*-type K^+, and *T*-type Ca^{2+} channels with reference to the base model (Fig. S1). Table S4 provides the parametric values for the new base model.

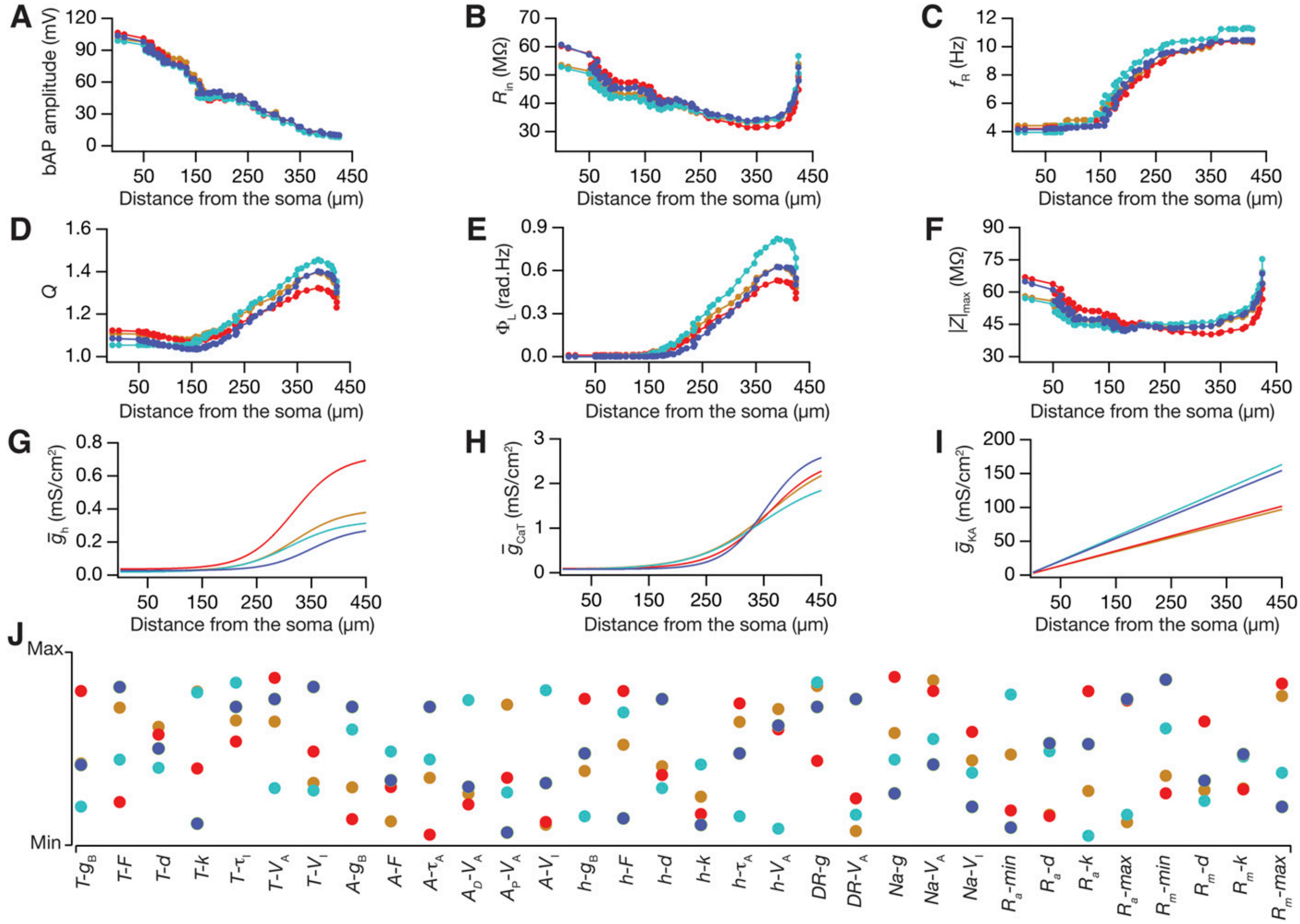

Fig. S5. In four randomly chosen valid models, analogous functional maps of all six measurements emerged in the absence of individual channelostasis in the underlying channel population. (*A*–*F*) Functional maps of back-propagating action potential (bAP) amplitude (*A*), input resistance (R_{in}) (*B*), resonance frequency (f_R) (*C*), resonance strength (*Q*) (*D*), total inductive phase (Φ_L) (*E*), and maximum impedance amplitude ($|Z|_{max}$) (*F*) represented along the somato-apical topograph of four valid models. (*G*–*I*) Distribution of *h* (*G*), CaT (*H*), and KA (*I*) conductances along the somato-apical trunk of the five valid models. (*J*) Distribution of all underlying model parameters in the five valid model neurons depicted along with their respective minimum–maximum range. Each colored circle represents parameters of the color-matched model depicted in *A*–*I*. Note that these valid models were obtained with global sensitivity analysis on the new base model (Fig. S4) and with parametric ranges provided in Table S5. A total of 9,000 random models were generated by uniformly sampling 32 parameters with ranges shown in Table S4 (same set of parameters as in Table S1 for the base model, but with different ranges to account for the new base model parameters). The validity of these randomly generated models was tested by comparing 18 measurements with their experimental counterparts (measurements and bounds are the same as before, in Table S3), and 27 models were declared valid.

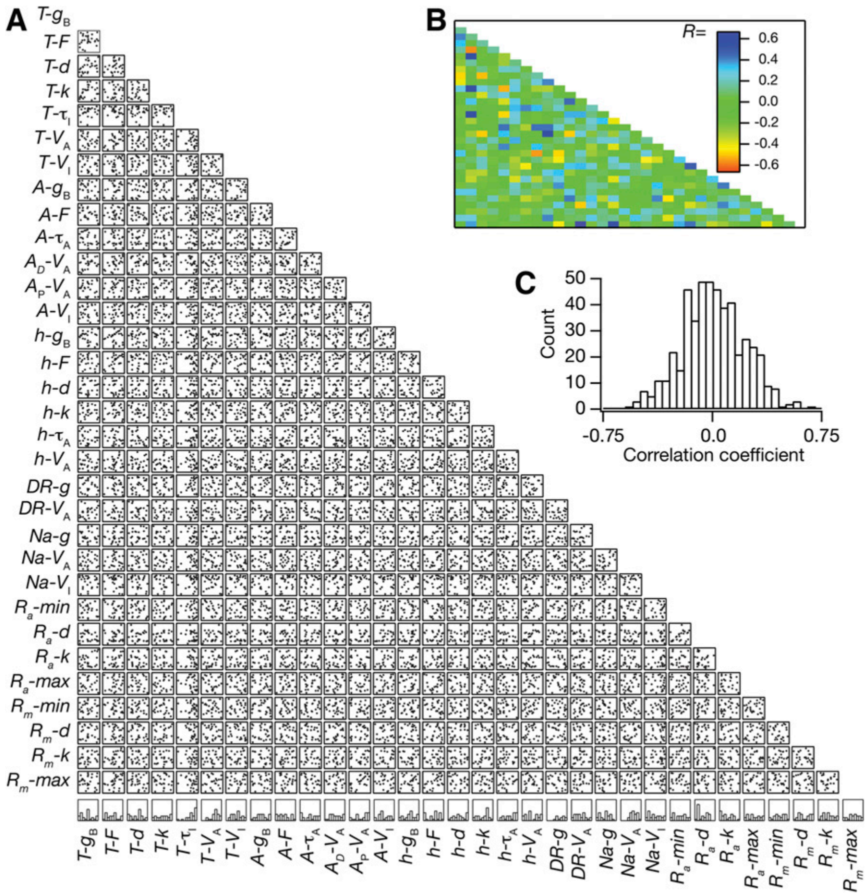

Fig. S6. Weak pairwise correlations between parameters underlying the new valid model population. (*A*) Lower diagonal of a matrix depicting interactions among the 32 parameters derived from all valid models obtained with the new base model (n = 27). Each subpanel depicts a scatter plot of the values of two parameters (labeled at bottom and at left) derived from all valid models. Correlation coefficients were computed for each of the scatter plots. The bottommost row denotes histograms of individual parameters in the valid model population. (*B*) Lower diagonal of a color-coded matrix of correlation coefficients corresponding to the scatter plots in *A*. (*C*) Distribution of correlation coefficients for the 496 pairs corresponding to the scatter plots in *A*. Note that the correlation coefficients span a larger range (compared with Fig. 4*C* for the base model) here because of the lower n (27 here vs. 228 in Fig. 4). We verified this by performing correlation analysis on 27 (randomly chosen) of the 228 valid models in Fig. 4 and found the range of correlation coefficients to match with that in *C*.

Table S1. Parameters, their default values, and testing ranges for generating randomized models

Count	Parameter	Symbol	Default value	Testing range
T-type Ca^{2+} channel properties				
1	Maximal conductance, μS/cm^2	T-g_B	55	40–70
2	Fold increase	T-F	25	20–30
3	Half-maximal point of g_{CaT} sigmoid, μm	T-d	370	330–410
4	Slope of g_{CaT} sigmoid, μm	T-k	15	5–25
5	Inactivation time constant, ms	T-τ_I	31.012	10–50
6	$V_{1/2}$ activation, mV	T-V_A	−60	−50 to −70
7	$V_{1/2}$ inactivation, mV	T-V_I	−85	−75 to −95
A-type K^+ channel properties				
8	Maximal conductance, mS/cm^2	A-g_B	3.1	2.6–3.7
9	Fold increase per 100 μm	A-F	5	4–6
10	Activation time constant KA, ms	A-τ_A	0.032	0.02–0.1
11	$V_{1/2}$ activation KA_{dist}, mV	A_D-V_A	−1	−5–5
12	$V_{1/2}$ activation KA_{prox}, mV	A_P-V_A	11	5–15
13	$V_{1/2}$ inactivation KA, mV	A-V_I	−56	−60 to −50
h channel properties				
14	Maximal conductance, μS/cm^2	h-g_B	40	30–55
15	Fold increase	h-F	20	15–25
16	Half-maximal point of g_h sigmoid, μm	h-d	370	330–410
17	Slope of g_h sigmoid, μm	h-k	14	10–20
18	Activation time constant of I_h, ms	h-τ_A	33.089	25–75
19	$V_{1/2}$ activation of I_h, mV	h-V_A	−82	−75 to −90
Delayed rectified K^+ channel properties				
20	Maximal conductance, mS/cm^2	DR-g	10	7–13
21	$V_{1/2}$ activation, mV	DR-V_A	13	5–20
Fast Na^+ channel properties				
22	Maximal conductance, mS/cm^2	Na-g	12.5	11–14
23	$V_{1/2}$ activation, mV	Na-V_A	−38	−30 to −45
24	$V_{1/2}$ inactivation, mV	Na-V_I	−50	−40 to −60
R_a distribution				
25	Minimum value, Ω·cm	R_a-min	10	5–15
26	Half-maximal point of R_a sigmoid, μm	R_a-d	320	300–340
27	Slope of R_a sigmoid, μm	R_a-k	14	10–20
28	Maximum value, Ω·cm	R_a-max	110	90–130
R_m distribution				
29	Minimum value, kΩ·cm^2	R_m-min	125	105–145
30	Half-maximal point of R_m sigmoid, μm	R_m-d	320	290–350
31	Slope of R_m sigmoid, μm	R_m-k	40	20–60
32	Maximum value, kΩ·cm^2	R_m-max	145	125–165

Table S2. Experimental measurements obtained from hippocampal CA1 pyramidal neurons

Location	bAP, mV	R_{in}, MΩ	f_R, Hz	Q	Φ_L, rad.Hz	$\|Z\|_{max}$, MΩ	n	Distance, μm
Soma	94.6 ± 0.77	73.1 ± 1.5	4.2 ± 0.06	1.23 ± 0.01	0.05 ± 0.004	86.9 ± 1.5	121	0
150 μm	59.2 ± 2.07	39.9 ± 2.9	4.0 ± 0.3	1.4 ± 0.1	0.2 ± 0.1	57.1 ± 2.7	17	143 ± 3.6
300 μm	26.4 ± 1.82	27.3 ± 2.8	7.1 ± 0.5	1.6 ± 0.1	0.6 ± 0.1	47.8 ± 3.7	15	283 ± 4.8

All data are presented as mean ± SEM. Number of experimental data points (*n*) and corresponding recording locations (Distance, μm) apply to all measurements except for bAP. Number of experimental data points and corresponding recording locations for bAP are as follows: 28 (soma), 35 (149.4 ± 6.5 μm), and 30 (262 ± 2.4 μm).

Table S3. Bounds for all 18 measurements for declaring a model to be valid

	Soma		~150 μm		~300 μm	
Measurement	Lower	Upper	Lower	Upper	Lower	Upper
bAP Amplitude, mV	90	105	40	70	10	25
Input resistance, R_{in}, MΩ	45	90	30	55	10	50
Resonance frequency, f_R, Hz	2	5.5	3	6.5	5	11
Resonance strength, Q	1.01	1.5	1.01	1.9	1.2	2.6
Total inductive phase, Φ_L, rad Hz	0	0.15	0	0.3	0.15	2
Maximum impedance amplitude, $\|Z\|_{max}$, MΩ	50	110	35	80	30	70

The bounds were fixed such that they cover ~80% of the experimental variability in the corresponding measurement (Fig. S1).

Table S4. Parameters, their default values, and testing ranges for generating randomized models

Count	Parameter	Symbol	Default value	Testing range
T-type Ca^{2+} channel properties				
1	Maximal conductance, μS/cm^2	T-g_B	**80**	**65–95**
2	Fold increase	T-F	**30**	25–35
3	Half-maximal point of g_{CaT} sigmoid, μm	T-d	**350**	**320–380**
4	Slope of g_{CaT} sigmoid, μm	T-k	**50**	**35–65**
5	Inactivation time constant, ms	T-τ_I	31.012	10–50
6	$V_{1/2}$ activation, mV	T-V_A	−60	−50 to −70
7	$V_{1/2}$ inactivation, mV	T-V_I	−85	−75 to −95
A-type K^+ channel properties				
8	Maximal conductance, mS/cm^2	A-g_B	3.1	2.6–4.5
9	Fold increase per 100 μm	A-F	**8**	**6–12**
10	Activation time constant KA, ms	A-τ_A	0.032	0.02–0.1
11	$V_{1/2}$ activation KA_{dist}, mV	A_D-V_A	−1	−5–5
12	$V_{1/2}$ activation KA_{prox}, mV	A_P-V_A	11	5–15
13	$V_{1/2}$ inactivation KA, mV	A-V_I	−56	−60 to −50
h channel properties				
14	Maximal conductance, μS/cm^2	h-g_B	**25**	**15–40**
15	Fold increase	h-F	**12**	**8–20**
16	Half-maximal point of g_h sigmoid, μm	h-d	**320**	**290–360**
17	Slope of g_h sigmoid, μm	h-k	**50**	**40–60**
18	Activation time constant of I_h, ms	h-τ_A	33.089	25–75
19	$V_{1/2}$ activation of I_h, mV	h-V_A	−82	−75 to −90
Delayed rectified K^+ channel properties				
20	Maximal conductance, mS/cm^2	DR-g	10	8–14
21	$V_{1/2}$ activation, mV	DR-V_A	13	5–20
Fast Na^+ channel properties				
22	Maximal conductance, mS/cm^2	Na-g	**16**	**14–23**
23	$V_{1/2}$ activation, mV	Na-V_A	−38	−34 to −42
24	$V_{1/2}$ inactivation, mV	Na-V_I	−50	−40 to −60
R_a distribution				
25	Minimum value, Ω·cm	R_a-min	**70**	**55–85**
26	Half-maximal point of R_a sigmoid, μm	R_a-d	**300**	**270–330**
27	Slope of R_a sigmoid, μm	R_a-k	**50**	**40–60**
28	Maximum value, Ω·cm	R_a-max	**120**	**100–140**
R_m distribution				
29	Minimum value, kΩ·cm^2	R_m-min	**85**	**70–100**
30	Half-maximal point of R_m sigmoid, μm	R_m-d	**300**	**270–330**
31	Slope of R_m sigmoid, μm	R_m-k	**50**	**30–70**
32	Maximum value, kΩ·cm^2	R_m-max	**125**	**110–140**

Default values and testing ranges of parameters in boldface type are different from those of the previous base model (compare Table S1).

Table S5. Number of virtual knockout models (VKMs) used for generating the histogram and calculating percentage change for a given measurement and for a given location

Location	*n* for bAP	*n* for R_{in}	*n* for f_R	*n* for Q	*n* for Φ_L	*n* for $\lvert Z \rvert_{max}$
Virtual *T*-type Ca^{2+} conductance knockout						
Soma	228	228	228	228	152	228
150 μm	228	228	228	228	173	228
300 μm	228	228	228	228	228	228
Virtual *h* conductance knockout						
Soma	228	214	214	214	134	214
150 μm	228	214	214	214	112	214
300 μm	228	214	214	214	214	214
Virtual *A*-type K^+ conductance knockout						
Soma	228	130	130	130	72	130
150 μm	228	130	130	130	26	130
300 μm	228	130	130	130	130	130
Virtual fast Na^+ conductance knockout						
Soma	228	228	228	228	143	228
150 μm	228	228	228	228	105	228
300 μm	228	228	228	228	228	228
Virtual delayed rectifier K^+ conductance knockout						
Soma	228	226	226	226	148	226
150 μm	228	226	226	226	172	226
300 μm	228	226	226	226	226	226

Consequent to low values of Φ_L at the soma and ~150 μm in certain models, the percentage change in Φ_L was very high after knocking out specific channels (infinity in some cases). These models were eliminated from analyses, leading to smaller *n* values for Φ_L. Similarly, some VKMs corresponding to KA channels were capable of sustaining intrinsic oscillations, leading to their elimination from further analyses.